A&A 431, 523–538 (2005)
DOI: 10.1051/0004-6361:20035746

Astronomy & Astrophysics

Physical conditions in Photo-Dissociation Regions around Planetary Nebulae⋆,⋆⋆

J. Bernard-Salas[1,2,3] and A. G. G. M. Tielens[1,2]

[1] SRON National Institute for Space Research, PO Box 800, 9700 AV Groningen, The Netherlands
e-mail: jbs@isc.astro.cornell.edu
[2] Kapteyn Astronomical Institute, PO Box 800, 9700 AV Groningen, The Netherlands
[3] Department of Astronomy, Cornell University, 219 Space Sciences Building, Ithaca, NY 14853, USA

Received 25 November 2003 / Accepted 1 October 2004

Abstract. We present observations of the infrared fine-structure lines of [Si II] (34.8 μm), [O I] (63.2 and 145.5 μm) and [C II] (157.7 μm) obtained with the ISO SWS and LWS spectrographs of nine Planetary Nebulae (PNe). These lines originate in the Photo-Dissociation Regions (PDRs) associated with the nebulae and provide useful information on the evolution and excitation conditions of the ejected material in these regions. In order to interpret the observations, the measured line intensities have been compared with those predicted by photo-dissociation models. This comparison has been done taking into account the C/O content in the nebulae. The densities derived with this comparison show a large scatter for some nebulae, probably because the density is higher than the critical density. Therefore, they are no longer sensitive to this parameter implying that transitions from other species with higher critical density should be used. The possible contribution of shocks to the observed emission characteristics of these PNe is briefly discussed and it is shown that the radiation field is the main driving force responsible for the atomic lines in the PNe that have been studied. In addition, data on the pure rotational lines of H_2 in three nebulae (NGC 7027, NGC 6302 and Hb 5) are also presented. Assuming local thermal equilibrium the rotational temperature and densities have been derived. We have derived the mass of atomic gas in the PDR associated with these PNe and compared those to ionic masses derived from Hβ and molecular masses derived from low J CO observations. This comparison shows that for these nebulae, the PDR is the main reservoir of gas surrounding these objects. A comparison of the results of these evolved PNe with very young PNe from the literature suggests that as the nebula ages the relative amount of ionic gas increases at the expense of the atomic and molecular mass.

Key words. ISM: lines and bands – ISM: atoms – ISM: molecules – ISM: planetary nebulae: general

1. Introduction

Planetary Nebulae (PNe) constitute one of the latest stages of evolution of intermediate mass stars (1–8 $M_\odot$). In the short-lived planetary nebula phase, the ionized gas is the result of the interaction of the previously ejected envelope with the far ultraviolet photons emitted by the hot (30 000–100 000 K) central star. The ultraviolet photons will photo-dissociate the molecules previously ejected. Then, as the stellar temperatures become higher some ionization will occur (Fong et al. 2001). This ionization gives rise to warm gas (10^4 K) which cools through the emission of copious amounts of FUV and visible line emission, which give these nebulae their optical prominence. Not all of the ejected envelope will be ionized and some atoms and molecules can survive this hostile environment. Neutral regions in the interstellar medium where the heating and chemistry are controlled by the penetrating far ultraviolet photons are called Photo-Dissociation Regions (PDRs). The infrared line emission of these regions consists mainly of the atomic fine structure transitions of [C I], [C II], [O I], and rotational lines of H_2 and CO, as well as the vibrational lines of PAH molecules.

Shocks can also photo-dissociate molecules, heat the gas and cause copious amounts of [C II] and [O I] emission. These shocks are the result of the interaction of the fast stellar wind, which dominates the late-AGB and/or the early post-AGB phase (Sahai & Trauger 1998), with the slow AGB wind. This interaction is very important since it shapes the nebula. However, recent studies show that the contribution from shocks in the emission of fine structure lines in PNe (often invoked in the past) seems to be less important (Hollenbach & Tielens 1999; Fong et al. 2001; Castro-Carrizo et al. 2001).

⋆ Based on observations with ISO, an ESA project with instruments funded by ESA Member States (especially the PI countries: France, Germany, The Netherlands and the UK) and with the participation of ISAS and NASA.

⋆⋆ Table 1 is only available in electronic form at the CDS via anonymous ftp to cdsarc.u-strasbg.fr (130.79.128.5) or via http://cdsweb.u-strasbg.fr/cgi-bin/qcat?J/A+A/431/523

The gas in the PDRs cools down via the far-infrared fine structure lines of [C II], [O I], [Si II], [C I] and molecules such as CO and H_2 (Tielens & Hollenbach 1985). The intensity of the cooling lines in the PDR depends on the conditions in these regions. The development of PDR models has put constraints on the physical parameters of the PDRs (namely the density and G_0[1]) by comparing the observations with the models. These models describe the chemistry and radiative transfer of the surface of molecular clouds (assumed as a plane-parallel semi-infinite slab) that are illuminated by far-ultraviolet photons (Tielens & Hollenbach 1985). They assume thermal balance and usually adopt the standard composition of the ISM.

The study of PDRs is of great importance for a proper understanding of the evolution of the ejected material, especially the excitation conditions under the influence of UV photons from the hot central nucleus. Measurements of the mass of the ionized gas in PNe (where PDRs have been detected) seem to indicate that, although the central stars in PNe are very hot, the mass found is several times lower than that of the neutral and molecular mass found in the PDRs (Hollenbach & Tielens 1999). As the nebula ages, the density drops and the amount of ionized gas increases. During the evolution of the PNe the atomic and molecular gas content varies, but it is not known how. Conversely, the presence of the atomic and molecular gas might influence the evolution of the PNe. Hints on these behaviours may well be reflected in the physical conditions or in the spectrum of such regions. This neutral and molecular gases, because of their low temperature, are not prominent in the optical or UV region. Therefore, the study of these regions must be carried out in the infrared.

The wavelength coverage and resolution of the SWS and LWS spectrometers on board ISO are ideal to study the lines originating in PDRs. They cover the spectral range in which these lines emit and have enough sensitivity to study PDRs in many PNe. Several studies have recently been reported: Liu et al. (2001); Fong et al. (2001); Castro-Carrizo et al. (2001). Liu et al. (2001) used LWS observations to derive ionic abundances of the ionized regions around 24 PNe, and the temperatures, densities and masses of the neutral gas in the PDRs. They found temperatures and densities of the studied PDRs ranging between 200–500 K and 400–6×10^5 cm^{-3}, and gas masses associated with the PDRs lower than 0.1 $M_\odot$. Fong et al. (2001) and Castro-Carrizo et al. (2001) used both LWS and SWS observations to investigate the fine structure lines from 12 carbon- and oxygen-rich evolved stars respectively and used PDR and shock models to compare to the observations. They found that photo-dissociation is the main driving force responsible for the observed lines and that the mass of the atomic gas grows as the nebula evolves.

Motivated by the results of Fong et al. (2001) and Castro-Carrizo et al. (2001) we decided to apply their analysis method to more PNe. We have selected a sample of nine PNe observed with ISO from which seven (except Hb 5 and K 3-17) were studied by Liu et al. (2001) using different methods. These measured atomic lines have been compared with existing PDR models to determine the conditions in the PDRs. We have extended their study of the line emission to the dust content of the nebulae as well. Emphasis has been put on deriving the ionized, atomic and molecular masses. These are combined with other evolved objects from the literature to provide an insightful view of the evolution of the different mass components in the nebula.

The plan of the paper is as follows. In the next two sections the observations are discussed and an explanation of the reduction analysis is given. This is followed by a general description of the PNe in the sample in terms of position in the sky, distance, diameter, extinction and C/O ratio. In Sect. 4 the SWS and LWS spectra are shown. In Sect. 5 the analysis of the atomic lines is described. These lines are compared with PDR models in Sect. 6. The possible presence of shocks is investigated in Sect. 7. The analysis and discussion of the hydrogen rotational lines found in three PNe are given in Sect. 8, where rotational temperatures and densities have been derived. Atomic, ionized and molecular masses are calculated in Sect. 9. A general discussion is given in Sect. 10. Finally in the last section the main conclusions of the paper are summarized.

2. Observations

The observations of the nine PNe presented in this study were taken with the two spectrographs on board ISO: The Short Wavelength Spectrometer (SWS) and the Long Wavelength Spectrometer (LWS). The observation numbers and exposure times are given in Table 1, available at the CDS and which contains the following information: Col. 1 lists the name of the source; Cols. 2 and 3 give the SWS on-source exposure number (TDT) and exposure time respectively; Cols. 4 and 5 give the LWS on-source exposure number and exposure time; Cols. 6 and 7 give the LWS off-source exposure number and exposure time. The observed spectrum for each PNe is shown in Fig. 2. The sample was selected to have high quality SWS and LWS full scan spectra. Both instruments are required to measure all the lines of interest. The full scan observation is needed to detect the dust features (when present) and to determine the integrated IR flux which is an essential parameter in model comparisons.

The SWS (de Graauw et al. 1996) covers the spectral range from 2.38 to 45.2 μm. The observation mode used in this work is AOT01. The SWS uses different size apertures for four different spectral regions. These apertures are $14'' \times 20''$, $14'' \times 27''$, $20'' \times 27''$ and $20'' \times 33''$ and relate to the wavelength intervals: 2.38–12.0 μm, 12.0–27.5 μm, 27.5–29 μm and 29.0–45.2 μm. The instrument has a spectral resolution ($\lambda/\delta\lambda$) that varies from 1000 to 2000. ISO pointing for these nebulae is adequate for all sources. However, we note that for NGC 3918 there was a mispointing of 14″ (Ercolano et al. 2003), and hence we may miss a large fraction of the SWS flux.

The LWS (Clegg et al. 1996) spectrograph covers the wavelength range from 43 to 196 μm. The observation mode used was AOTL01 and provides a resolution that varies (depending on wavelength) from 140 to 330. The aperture of the LWS is 80″. Both observations (SWS and LWS) were pointed at the

[1] G_0 is the incident far-ultraviolet flux between 6 and 13.6 eV in units of the average interstellar radiation field.

Table 2. General parameters of the PNe. The m_V is not corrected for extinction. See text (Sect. 3) for details on the adopted diameters.

Name	Label	$l(^\circ)$	$b(^\circ)$	dis (pc)	diam ($''$)	m_V (mag)	E_{B-V}	[C/H] $\times 10^{-4}$	Type (C/O)†
NGC 7027^{d1,t1,m1,e1}	1	84.93	−3.50	650	16	16.53	0.85	5.1	C-rich (1.3)
NGC 6153^{d2,t2,m1,e2}	2	341.8	5.44	1700	25	15.55	0.81	6.8	O-rich (0.8)
BD+30 3639^{d3,t3,d4,e3}	3	64.79	5.02	1200	7	11.80	0.34	7.3	C-rich (1.6)
NGC 3918^{d4,t4,m1,e4}	4	294.7	4.71	1000	10	15.49	0.30	8.0	C-rich (1.6)
Hb 5^{d5,t5,d4,e5}	5	359.4	−0.98	2000	4	14.60	1.05	4.0	C-rich ?
Mz 3^{d6,t6,d4,e6}	6	331.7	−1.06	1300	1	14.10	1.25	4.0	O-rich ∼1
K 3-17^{d6,d4}	7	39.83	2.17	1500	8			4.0	C-rich ?
NGC 6543^{d7,t7,m1,e3}	8	96.47	29.95	1000	15	11.29	0.07	2.5	O-rich (0.4)
NGC 6302^{d8,t8,m2,e7}	9	349.5	1.06	1600	10	18.90:	0.88	0.6	O-rich (0.3)

References: ^{d1}Bains et al. (2003); ^{d2}Average of Pottasch (1983) and Sabbadin (1986); ^{d3}Li et al. (2002); ^{d4}Acker et al. (1992); ^{d5}Sabbadin (1986); ^{d6}Cahn et al. (1992); ^{d7}Reed et al. (1999); ^{d8}Terzian (1997); ^{t1}Kastner et al. (1996); ^{t2}Liu et al. (2000); ^{t3}Hora et al. (1993); ^{t4}Corradi et al. (1999); ^{t5}Phillips & Mampaso (1988); ^{t6}Quinn et al. (1996); ^{t7}Latter et al. (1995); ^{t8}Persi et al. (1999); ^{m1}Ciardullo et al. (1999); ^{m2}Assumed; ^{e1}Bernard Salas et al. (2001); ^{e2}Pottasch et al. (2003); ^{e3}Bernard-Salas et al. (2003); ^{e4}Clegg et al. (1987); ^{e5}Erwin Platen (private communication); ^{e6}Cohen et al. (1978); ^{e7}Beintema & Pottasch (1999).

† C/O ratio taken from the same references as the extinction except for Mz 3 where the ratio is given by Zhang & Liu (2002).

: Large error.

center of the nebulae (see Table 2 for coordinates). The pointing errors for ISO are ∼1.5″.

2.1. Reduction techniques

The tools used to reduce the SWS data can be found in the interactive analysis software package which is distributed by the SWS consortium, *IA3* (de Graauw et al. 1996). The reduction procedure follows that of Bernard-Salas et al. (2003) (to which we refer for further details) and here only some peculiarities are mentioned.

If memory effects were present, the tool *dynadark* (Kester 2001) which minimizes these effects was applied. The spectra were rebinned to a fixed resolution which depends on the mode (speed) of the observation. Occasionally some different bands exhibit an offset with respect to the overall spectrum due to the dark current. This has an additive effect in the spectrum and was corrected by applying a shift of several Jy to match the other bands. This was the case for BD+30 3639, Hb 5 and NGC 6302 in band *3E* and for NGC 6543 in bands *3A* and *4*. The offsets applied (always positive) were respectively 35, 15, 140, 55 and 5 Jy.

The reduction of the LWS resembles that of the SWS and was done using the Spectroscopy Analysis Package (ISAP). Scan 7 is corrupted and was always removed. Glitches and bad data were also rejected. In the next step the spectrum was averaged at a fixed resolution and finally the fringes, if present, were removed.

3. General parameters of the PNe

In Table 2 some useful information on the PNe and adopted parameters relevant to this study are given. In the first column the PNe are labeled with a number for identification in Figs. 3–6, 9, and 10. References to the distances, diameters, magnitudes in V and extinctions are indicated by the superscripts *dx, tx, mx, ex* respectively and are given as a footnote to the table.

The galactic coordinates in Cols. 3 and 4 show that all the objects are in the disk, except NGC 6543 which is ∼30° above the galactic plane. The adopted distances range from 650 to 2000 parsecs and these PNe are therefore close objects. The reader should bear in mind that distances to PNe are very difficult to determine and therefore very uncertain. It is common (unfortunately) to find distances in the literature for the same object that differ by a factor of two or sometimes even more. Great care was taken in adopting the most reliable values for the distances. From the different methods we favor the expansion velocity distances when available above other methods. The diameters in which we are interested are those of the PDR, which sets the value of the Far-Ultraviolet (FUV) radiation field incident on the PDR. This can be traced very well with H_2 images since this molecule peaks close to the surface of the PDR. Near and mid infrared continuum images are also good indicators because the dust emission is located at the inner edge of the PDR. Moreover, we expect the PDR to have a thickness which is small compared to the size of the ionized gas. Hence, for reasonable geometries, the emitting surface can be estimated from this size as well. Radio and optical images provide a good estimate of the H II region, thus providing lower limits to the actual PDR size. For those reasons H_2 images were preferred, then infrared and when not available either radio or optical were used. The adopted diameters in Col. 6 correspond to: H_2 images in NGC 7027, BD+30 3639, NGC 6543, NGC 6302, a 10 μm image for Mz 3, radio images for Hb 5 and K 3-17, and optical images for NGC 6153 and NGC 3918.

The V magnitudes are given in Col. 7. For NGC 6302 the magnitude is *assumed* since the central star has not yet been seen. The case of K 3-17 was more troublesome because the extinction is not known and no magnitude was assumed. The extinction (Col. 8) for the remaining nebulae is in most cases low. The measured lines for K-3 17 (O I and C II) could not be corrected for extinction but the correction for extinction in these infrared lines is very small and is within the absolute flux errors. The adopted carbon abundance is given in Col. 9. Finally, in the last column, the carbon or oxygen rich nature of the

Table 3. Radius, Zanstra temperature and luminosity of the observed PNe. $F(\mathrm{H}\beta)$ and $F(4684$ Å$)$ are in units of 10^{-12} erg cm^{-2} s^{-1} (not corrected for extinction). The central star radius is in meters.

Name	Hydrogen				Helium			
	$F(\mathrm{H}\beta)^{\dagger}$	Radius	$\log(\frac{L_*}{L_\odot})$	$\log T_Z(\mathrm{H})$	$F(4686$ Å$)^{*}$	Radius	$\log(\frac{L_*}{L_\odot})$	$\log T_Z(\mathrm{He})$
NGC 7027	75.9	2.72E+07	3.31	5.29	31.10	2.76E+07	3.27	5.28
NGC 6153	13.8	1.90E+08	3.18	4.84	2.74	1.58E+08	3.56	4.97
BD+30 3639	93.3	5.45E+08	3.14	4.60				
NGC 3918	91.2*	3.92E+07	2.85	5.10	14.60	4.05E+07	2.77	5.07
Hb 5	3.02*	7.58E+08	3.20	4.54	1.54	4.49E+08	4.17	4.90
Mz 3	8.13*	7.36E+08	3.46	4.62				
K 3-17								
NGC 6543	245.5	3.67E+08	2.96	4.64	14.70	2.81E+08	3.46	4.82
NGC 6302:	29.5	1.77E+07	3.86	5.52	16.60	1.76E+07	3.88	5.53

: Large error in the radius, temperature and luminosity.
† From the same references as the extinction in Table 2, otherwise indicated.
* From Acker et al. (1992).

nebulae is stated by means of the C/O ratio. This is important in order to compare these objects with the appropriate PDR models. For Hb 5 and K 3-17 the C/O ratio is not known, and in Mz 3 is very close to 1 (Zhang & Liu 2002). Their C- or O-rich nature was established by looking at the dust features in the spectrum (Table 4). PAH features, present in C-rich environments, were found in Hb 5 and K 3-17. On the other hand silicate features are present in the spectrum of Mz 3 which indicates an O-rich environment. While this method has been used before, it is not a foolproof method since, for instance, some sources show both PAH and silicate features (see NGC 6302 and BD+30 3639 in Table 4). BD+30 3639 needs special attention. This nebula has been assumed in this study to be carbon-rich (based on the C/O ratio), but probably the bulk of the cold dust is oxygen-rich. Whether the PDR lines are formed mostly in the carbon- or oxygen-rich part of the shell is unknown. In either case, the results of our analysis and conclusions for this nebula would not have changed assuming that it is oxygen-rich.

In order to relate the analysis of the data with the evolutionary status of the central star, the Zanstra temperatures (T_Z), radii and luminosities have been derived (Table 3) using the data in Table 2 and the Hβ and helium λ4686 Å fluxes. The effect of over-estimating T_Z in the case of hydrogen and under-estimating it when using helium (Stasińska & Tylenda 1986) has been corrected. Further details of this correction can be found in Stasińska & Tylenda (1986) and Marigo et al. (2003). Since the nebula is probably thick for helium ionizing photons, T_Z(He) was preferred.

The results are shown in Fig. 1. For those objects where no helium line is detected the results using T_Z(H) have been plotted. For K3 17 no Hβ or helium λ4686 Å lines have been detected and therefore this object is not shown. The evolutionary tracks of Vassiliadis & Wood (1994) are related to the core mass rather than the initial mass to avoid the uncertainty in the mass loss. Stars with different initial mass and different mass loss functions can lead to the same core mass. While this figure may provide some insight into core mass and time evolution of these objects, the many uncertainties (especially in distance)

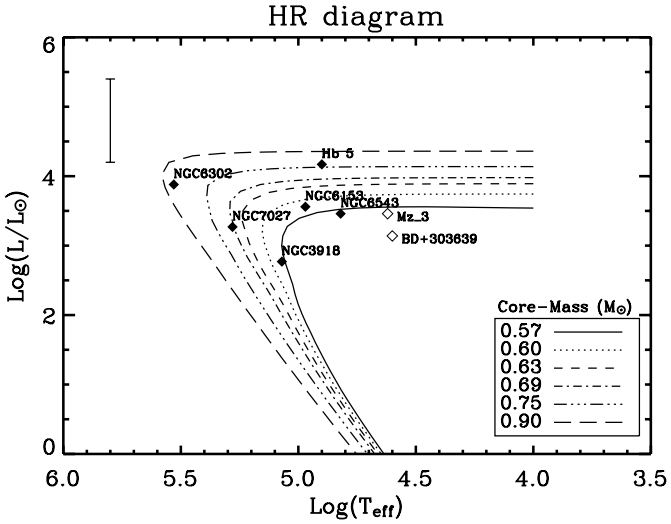

Fig. 1. HR diagram for the PNe of the sample. The $T_{\rm eff}$ have been derived with the Zanstra method using the helium lines (filled diamonds) and Hβ line (open diamond). The hydrogen-burning post-AGB evolutionary tracks from Vassiliadis & Wood (1994) are also plotted for different core masses, indicated in the lower-right corner of the figure. In the upper-left corner the uncertainty in the luminosity due to the error of a factor two in the distance is shown.

should be born in mind. NGC 3918 is in the last stage of the PNe phase while Mz 3 seems to be the youngest one in the sample. NGC 6302 and NGC 7027 have very hot central stars which translates into a very rich emission line spectra (Fig. 2). BD+30 3639 falls somewhat outside the range of the theoretical curves. Since this PN is powered by a WC central star nucleus, this may reflect its non-standard evolutionary history.

4. The SWS and LWS spectra

The complete SWS and LWS spectra are shown in Fig. 2. The strong forbidden lines which dominate the spectra have been cut to highlight the dust features. They are ordered such that

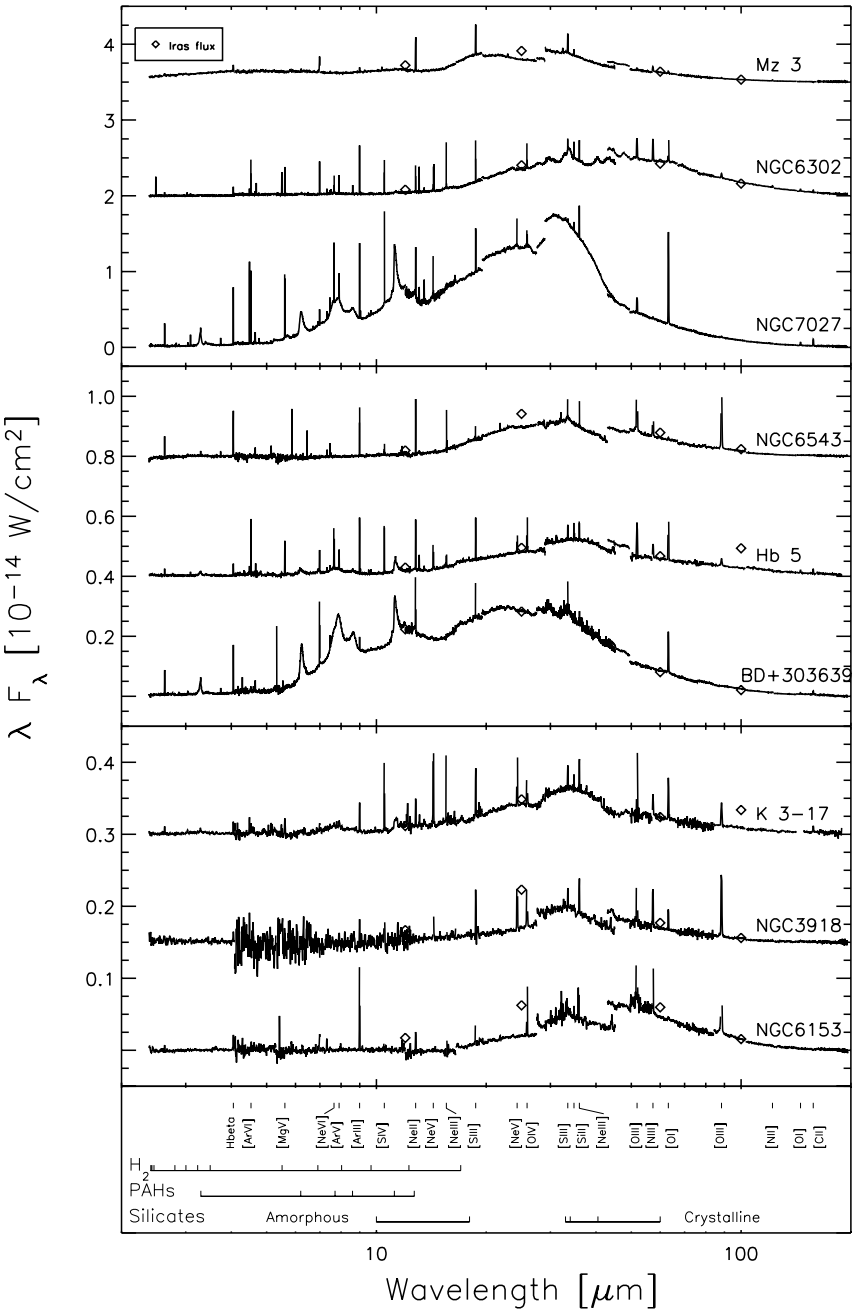

Fig. 2. SWS and LWS spectra. See Sect. 4 for details.

the continuum emission is largest in the top panel and lowest in the bottom one. In each panel the two upper spectra have been scaled with respect to the bottom one. In particular the fluxes of NGC 6302 and Mz 3 were shifted by 2 and 3.5×10^{-14} W cm^{-2} respectively. Those of Hb 5 and NGC 6543 by a factor 4 and 8×10^{-15} W cm^{-2}. Finally NGC 3918 and K 3-17 were shifted by a factor 1.5 and 3×10^{-15} W cm^{-2} respectively. The IRAS fluxes at 12, 25, 60 and 100 μm are also shown. The calibration error of the IRAS fluxes vary from ~20 to ~40%. Calibration errors on the ISO spectra are lower, ~10 to ~15%. The agreement of the IRAS fluxes with the ISO spectra is good for most cases but for some of them there are big discrepancies. The discrepancies seen in NGC 3918 likely reflect the already mentioned mis-pointing of the ISO observations, which is missing some of the flux. NGC 6543 is larger in size than the SWS apertures which implies that we are missing a factor of 2 in the region from 2.4–12 μm (Bernard-Salas et al. 2003). NGC 6153's size (see Table 2) is also bigger than the SWS apertures and some flux must have been missed in the SWS measurements. The disagreements at 100 μm in K 3-17 and Hb 5 are hard to explain since we are sure that the LWS aperture contains the whole nebula in both cases as can be seen from the 60 μm fluxes which agree well with the LWS data. Even the 12, 25 IRAS μm fluxes match the ISO-SWS data. For these reasons we decided to rely more on the ISO fluxes.

For the sake of clarity in Fig. 2 the most prominent forbidden lines, molecular lines and dust features (PAHs and

Table 4. Presence of PAH and silicate features in the spectra.

Name	PAH features (μm)						Silicate features	
	3.3	6.2	7.7	8.6	11.2	12.7	Amorphous	Crystalline
NGC 7027	√	√	√	√	√	√		
NGC 6153							√?	?
BD+30 3639	√	√	√	√	√	$\surd^{w}$		√
NGC 3918								
Hb 5	√	√	√	√	√	?		?
Mz 3							√	√
K 3-17$^{\sharp}$	$\surd^{w}$				√			
NGC 6543							√	√
NGC 6302	√	√	√	√	√		√?	√

$^{\sharp}$ Noisy spectrum.
^{w}: Weak feature. √?: Not clear, but probably present. ?: Dubious.

silicates) have been labeled at the bottom. The line emission in NGC 7027, NGC 6302, BD+30 3639, Hb 5, and NGC 6543 is stronger and more lines are observed than in Mz 3, K 3-17, NGC 6153 and NGC 3918. The last three present a very low continuum as well, hardly any dust features and few lines up to 10 μm. In Table 4 the presence or absence of dust features (those labeled at the bottom of the figure) is indicated. In BD+30 3639 it is difficult to confirm the presence of the 18 μm amorphous silicate feature because there is additional structure on top of it (Molster, private communication). Since the 10 μm region in BD+30 3639 is PAH dominated we therefore think that no amorphous silicates are present. The SWS spectrum of NGC 3918 is very noisy from 4 to 12 μm and no dust features are seen in that spectral region. However, Hony et al. (2002b) showed the presence of the 30 μm dust emission feature due to MgS. The PAH features in NGC 7027 and BD+30 3639 and the crystalline silicates of NGC 6302 and BD+30 3639 are easy to spot. Except for NGC 6302 and BD+30 3639, the PNe that show PAH features do not show silicates and vice-versa.

5. Line fluxes

5.1. Analysis of the atomic lines

The atomic lines originating in PDRs include [Si II] at 34.8 μm, [O I] at 63.2 and 145.5 μm, and [C II] at 157.7 μm. The observed fluxes for these lines are shown in Table 5. The [Si II] line is measured with the SWS and the lines of [O I] and [C II] with the LWS. The error on the fluxes are 15–20% for the Si II and ∼10% for the rest. The only exceptions are the C II line in NGC 6302 with an error of 25% and the two lines labeled noisy in Table 5 with an error ∼50%. The measurements made with the LWS could be background contaminated because of its large aperture and considering that PNe are compact objects. For that reason OFF observations were used to correct for this effect. The background could contribute to the C II line and to a lesser extent to the [O I] (63.2 μm) line. Those lines affected by background emission are labeled with a *B* in the Table. In these cases the background flux was subtracted from that of the source. These fluxes were then corrected for extinction (see Table 2, Col. 8) using the extinction law of Weingartner & Draine (2001). Since the models predict the intensities, the de-reddened fluxes were divided by the solid angle of the PDR for a proper comparison.

Table 5. Atomic line fluxes in units of 10^{-12} erg cm^{-2} s^{-1}. The background contribution (if present) in the LWS has been subtracted.

Name	Si II 34.8 μm	O I 63.2 μm	O I 145.5 μm	C II 157.7 μm
NGC 7027	14.34	601.0	20.4	36.0
NGC 6153	4.84	3.73		
BD+30 3639		70.9	2.16	5.11
NGC 3918		14.41	0.43:	0.57^{B}
Hb 5	14.16	89.3^{B}	4.89	5.10^{B}
Mz 3	23.4	14.2^{B}	1.18	
K 3-17$^{\natural}$	5.90	29.9	1.22	4.55^{B}
NGC 6543	1.39	3.95		0.45:
NGC 6302	20.4	268.1	12.8	11.19^{B}

: Noisy line.
$^{\natural}$ Not corrected for extinction.
^{B} These lines were background contaminated.

For the seven PNe in our sample that were also studied by Liu et al. (2001) (all except Hb 5 and K 3-17), the measured fluxes agree within errors (∼10%) to those quoted by them. The only exceptions are; the 63.2 μm line in NGC 6153 and NGC 6543, the 157 μm flux in NGC 7027, and the 146 μm flux in BD+30 3639. In these cases the difference is ∼15%, which is fairly good considering that the calibration files used in both studies are different. Liu et al. (2001) used OLPv7.0 and in this paper the OLPv9.5 was used.

5.2. Background contamination and aperture corrections

No LWS OFF-source observations were available for NGC 7027, BD+303639 and NGC 6543 (see Table 1). In order to estimate whether there is contribution from the ISM in these sources we proceeded as follows. In the case of NGC 7027 two LWS04 observations were available (TDT = 53001056 ON-source and TDT = 53001057 OFF-source). This mode of observation provide a high resolution Fabry-Pérot spectrum around small wavelength intervals, including the ones of interest. The OFF-source observation revealed that there is no

background contribution to the fine structure lines. The lines in the ON-source spectrum were measured and agreed within errors with the grating fluxes listed in Table 5. Although the LWS04 observation provides high resolution, the LWS01 was preferred. This is because the small wavelength interval in the LWS04 observation mode makes it difficult to establish the base line for the continuum. NGC 6543 is at 30° of the galactic plane (Table 2) and at those latitudes no contribution from the ISM is expected. IRAS maps at 12 and 100 μm show that there are no sources close by and therefore we conclude that there is no background contamination. The last PN, BD+30 3639, lies at 5° from the galactic plane and an ISM contribution could be expected. Again IRAS (at 100 μm) and MSX maps indicate that there are no sources in the vicinity of this PN. However, the [C II] line is observed all over the galactic plane. For the rest of the paper, we have assumed that this bright nebula is not affected by background contamination and we shall give less weight to the results derived from the [C II] line. The adopted fluxes of Mz 3 by Liu et al. (2001) are not corrected for background emission. They claim that the LWS-OFF source is contaminated by a bright H II region and adopted the ON source fluxes. In this article we have subtracted the OFF observation and, as the reader shall see later, this does not affect our conclusions since the intensities derived for Mz 3 are larger than those predicted by PDR models. The diameter of the PDR in NGC 6153 (25″) is slightly larger than the SWS aperture in which the [Si II] 34 μm line (20″ × 33″) was measured. The continuum is low in this nebula but IRAS fluxes (see Fig. 2) at 12 and 25 μm indicate that the SWS is missing ∼10 and 30 Jy respectively at those wavelengths. Since the continuum increases at longer wavelengths (up to 40 μm) it is likely that we are missing flux in the [Si II] line in NGC 6153. To convert the observed flux of this line into intensity we divided in this case by the beam size instead of the PDR size. When comparing this line to PDR models we will assign more weight to the analysis of the [O I] line. The LWS encompasses all of the PDR.

6. Physical conditions of the PDRs

The fine structure line fluxes shown in Table 5 are in this section compared to PDR models in order to derive the gas properties of these regions.

6.1. G_0 and the FIR flux

The intensity of the lines predicted by the PDR models depends on the relative strength of the incident FUV flux, indicated by G_0. This parameter has been derived assuming that all the UV photons are absorbed in a (spherical) shell of the size of the PDR and re-emitted in the infrared continuum. G_0 has been normalized to the average interstellar UV field (1.6×10^{-6} W m^{-2}; Habing 1968). The formula used is:

$$G_0 = \frac{4\ F_{\rm IR}}{1.6\ 10^{-6} \times 2.35\ 10^{-11}\ \theta^2}. \quad (1)$$

In Eq. (1), θ is the diameter of the PDR (see Table 2) in arcseconds and $F_{\rm IR}$ is the observed infrared flux in W m^{-2}. This latter quantity has been calculated integrating the SWS and LWS spectra of Fig. 2. The error in $F_{\rm IR}$ is less than 15%. As explained in Sects. 4 and 5 some flux was missed in the SWS spectra of NGC 3918, NGC 6153 and NGC 6543. For these nebulae we adopted the $F_{\rm IR}$ given by Pottasch (1983) using the IRAS fluxes. The $F_{\rm IR}$ and G_0 are listed in the second and third column of Table 6.

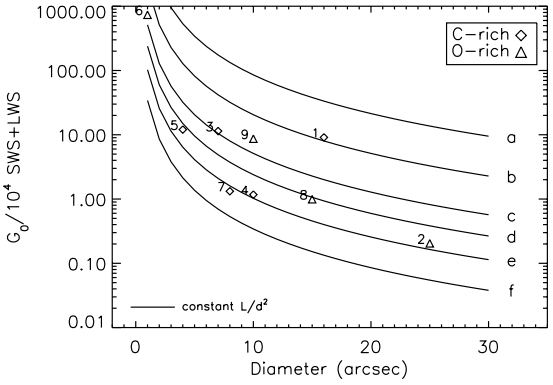

Fig. 3. G_0 versus diameter of the nebulae. The solid lines represent theoretical G_0 at a given diameter for different luminosities and distances where a, b, c, d, e and f correspond to L/d^2 ratios (in W m^{-2}) of 100, 24, 6, 2.8, 1.2 and 0.4 respectively.

The G_0 values have been plotted versus the diameter in Fig. 3. There is an obvious trend of decreasing G_0 with increasing diameter as is expected. The theoretical flux densities of a nebula with different diameters and for a given luminosity and distance are shown as solid lines for comparison. This is calculated by substituting $F_{\rm IR}$ by $L/(4\pi d^2)$ in Eq. (1), with L the luminosity and d the distance to the object.

6.2. Comparison with PDR models

The comparison has been divided according to the carbon- or oxygen-rich nature of the objects (Table 2, Col. 10). This has been possible thanks to the recent development of PDR codes especially developed for carbon rich gas (Latter 2004, in preparation). Previous models were created to interpret the interstellar medium which is oxygen rich. The models used in this paper are those of W. Latter reported in Fong et al. (2001) for the carbon rich nebulae, and those by Kaufman et al. (1999) for the oxygen rich objects. The C/O ratios used in the models of Fong et al. (2001) and Kaufman et al. (1999) are respectively 3.0 and 0.47. Although these ratios might not be representative for all the nebulae they are valid for a general comparison with the observations since our nebulae are typically within a factor of 2 of either the oxygen-rich or the carbon-rich C/O ratios used in the models.

A comparison of the observed intensities with those predicted by the PDR models at different G_0 and densities is shown in Fig. 4. The observational line data has been plotted adopting the G_0 values derived in Sect. 6.1. We recall that the numbers in these plots refer to the names of the objects in Table 2. The densities derived from this comparison for different species are given in Cols. 3 to 6 in Table 6. Some conclusions can be drawn from this comparison: 1) there are some objects that lie outside

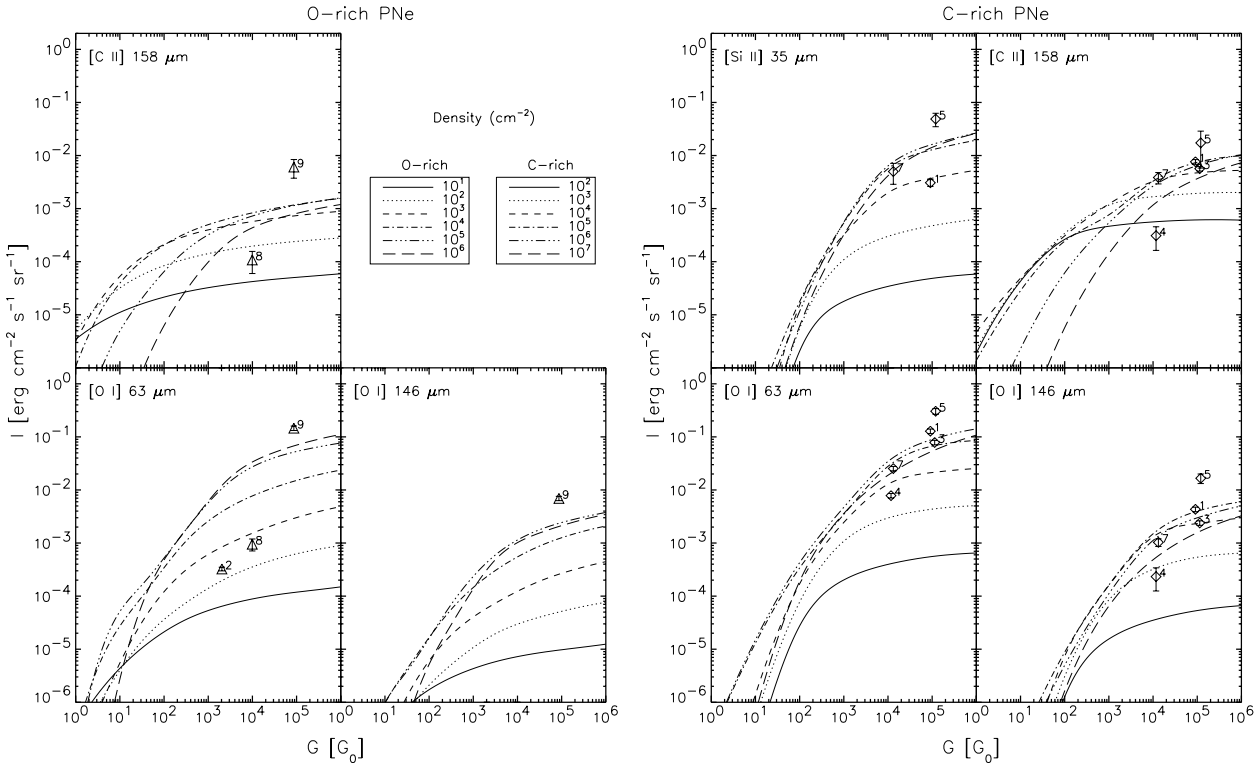

Fig. 4. Comparison of the atomic fine structure line fluxes and the incident flux density of the oxygen- and carbon-rich PNe with the theoretical PDR models of Kaufman et al. (1999) and W. Latter as reported in Fong et al. (2001). The error in G_0 is approximately of the size of the plotted symbols. Note that the oxygen-rich PN Mz 3 is not plotted because it lies outside the model predictions for G_0. The intensities of the oxygen lines for Mz 3 (the carbon line is not observed) are also higher than those predicted by the models.

Table 6. Far infrared flux, incident FUV flux G_0 (normalized to the average interstellar field) and density $n_{\rm H}$ (in cm^{-3}) of the nebulae. See text for details.

Name	$F_{\rm IR}$	G_0	$n_{\rm H}$ (cm^{-3})				Grid models	
	(W m^{-2})	(1.6e-6 W m^{-2})	Si II	O I (63 μm)	O I (146 μm)	C II	G_0	$n_{\rm H}$ (cm^{-3})
NGC 7027	2.2×10^{-10}	9.1×10^{4}	10^{4}	F	$>10^{5}$	$>10^{5}$	2×10^{5}	$>10^{7}$
NGC 6153	1.2×10^{-11}	2.0×10^{3}		2×10^{2}				
BD+30 3639	5.3×10^{-11}	1.1×10^{5}		$>10^{5}$	$>10^{4}$	$>10^{4}$	8×10^{5}	$>6\times10^{5}$
NGC 3918	1.1×10^{-11}	1.2×10^{4}		9×10^{3}	$>10^{3}$	F	1×10^{6}	$>10^{7}$
Hb 5	1.8×10^{-11}	1.2×10^{5}	F	F	F	F	10^{5}	$>2\ 10^{5}$
Mz 3	6.9×10^{-11}	7.3×10^{6}	F	F	F			
K 3-17	7.9×10^{-12}	1.3×10^{4}	$>2\times10^{4}$	$>10^{5}$	$>5\times10^{3}$	$>10^{4}$	10^{5}	5×10^{4}
NGC 6543	2.1×10^{-11}	9.9×10^{3}		8×10^{2}		$>5\times10^{1}$	4×10^{5}	4×10^{3}
NGC 6302	8.2×10^{-11}	8.7×10^{4}		F	F	F	6×10^{4}	3×10^{4}

F: Models do not reproduce the observations.

the range predicted by the models. This is the case for Hb 5, NGC 6302 and Mz 3. This could point to a problem in the models but it might be related to the adopted diameter, meaning that it has been under-estimated. This could certainly be the case for Hb 5 because the PDR size was estimated from a radio image. On the other hand the size of the PDR in NGC 6302 and Mz 3 were deduced from a 2.1 μm molecular image and a 10 μm image respectively and they should be quite reliable. The PDR size in Mz 3 is even more puzzling since it leads to a very high value of G_0 while it has the coolest central star of the sample. 2) The densities derived from different species for a given object show a factor of 10 difference in some cases. This is difficult to link to uncertainties in the observations because the error in the fluxes are small. The explanation might lie in the critical density. Probably the densities in these regions are higher than the critical density for these lines. This implies that the populations of the levels can be described with a Boltzmann distribution which is no longer dependent on the density but on the temperature. Therefore, in many cases only lower limits could be given. In Sect. 3, a carbon-rich nature was assumed for BD+30 3639 based upon the nebular C/O ratio but this is not entirely clear since the composition of the dust might be oxygen-rich for this nebula. Moving BD+30 3639 in Fig. 4 from the carbon-rich panel to the oxygen-rich would have led

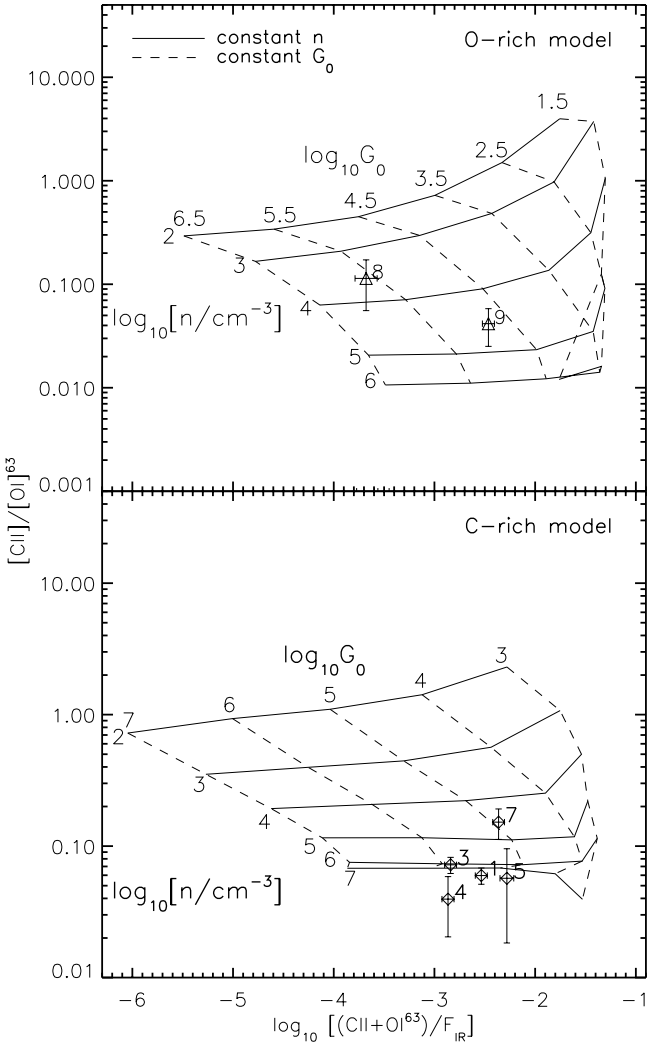

Fig. 5. *Top panel*; comparison of the O-rich model by Kaufman et al. (1999) (dashed and solid lines) with the observational points (triangles). *Bottom panel*; same as the top panel but comparing the C-rich model of W. Latter as reported in Fong et al. (2001) with the observational points (diamonds).

to the same conclusions in this nebula. The models fail to reproduce the carbon intensity and from the [O I] plots virtually the same upper limits for the density would have been derived.

In Fig. 5 we compare the data to the models using the [C II]/[O I] ratios and the ratio of the ([C II]+[O I]) to the $F_{\rm IR}$ dust continuum. The former ratio is a good indicator of density over the range $\sim 10^3$–10^6 cm^{-3}. The latter ratio essentially compares the cooling of the gas to the emission by the dust: this is therefore just a measure of the coupling efficiency of the gas to the FUV photon field through the photo-electric effect working on small dust grains and PAH molecules. These figures provide a very convenient way of comparing the observations and the models. The advantage of using ratios is that the uncertainty in the size of the PDR cancels. Furthermore both G_0 and the density can be derived simultaneously. These are shown in the last two columns of Table 6. The oxygen-rich models give a reasonable indication of these parameters in the oxygen-rich PNe NGC 6543 and NGC 6302 because the population of the levels is still not thermally populated. Nevertheless the G_0 in the former is larger than that derived using Eq. (1) which is probably more accurate. The carbon-rich nebulae are all clumped in the region of high density predicted by the models. In that region it is difficult to assess the density because it is outside of the range of the critical densities of the lines used. The incident FUV flux density derived with these figures agrees in general with those derived by integrating the infrared spectrum (Col. 3 in Table 6).

The comparison demonstrates that although these models can – and have been used in the past – to distinguish between PDRs in different circumstellar environments (including PNe), they cannot be used to reliably derive the density in PNe because in many cases the density exceeds the critical one. We conclude that in order to determine the density using these models, other species with higher critical densities must be used. In that respect, high level CO lines might be good tracers and these have been successfully used by Justtanont et al. (2000) for NGC 7027. Their best fit PDR model compared to their observed CO lines intensities gives a density of 10^6 cm^{-3}.

Considering the different uncertainties that affect each method we conclude that the G_0 in Col. 3 of Table 6 is the most accurate since it is calculated directly by integrating the IR spectrum and the main error comes from the adopted diameters. For the oxygen rich nebulae the G_0 and densities derived in Fig. 5 (Col. 8) seem very reliable as well. This representation has the advantage that it does not depend on the diameter but of course it is subject to assumptions in the models (i.e. elemental abundances and the photo-electric heating of O-rich nebulae). For the carbon rich nebulae the picture is more problematic. Figure 5 does not give a good estimate of the density except for K 3-17. Figure 4 is not exempt from problems when deriving the density but using the [O I] at 63.2 μm is probably the best estimate we can get, since this line is the strongest and is more accurately measured.

The comparison of our detailed model analysis of the PDR lines and the analysis by Liu et al. (2001) shows agreement within a factor 10 for the derived densities. In some cases (BD+30 3639, NGC 6543 and NGC 6302) the agreement is particularly satisfactory and shows that simple analysis of PDR lines provides a reliable tool to derive the physical conditions of the emitting gas (see also Wolfire et al. 1990).

7. PDRs versus shocks

In the introduction we mentioned that shocks are also able to photo-dissociate and heat the gas. This mechanism is thought no to be very important in PNe (Hollenbach & Tielens 1999). Indeed, the results by Fong et al. (2001) and Castro-Carrizo et al. (2001) show that photo-dissociation is the dominant process in the circumstellar envelope in the PNe that they studied. There are two kind of shocks, C-shocks (continuous or magnetic) and J-shocks. In the former molecules are not dissociated or species ionized. J-shocks on the other hand are more violent. Molecules are readily dissociated and (for high velocities) the gas is ionized. See van den Ancker (1999) for more details.

The intensity of the cooling lines is different in photo-dissociated gas than in shocked gas. Comparison of

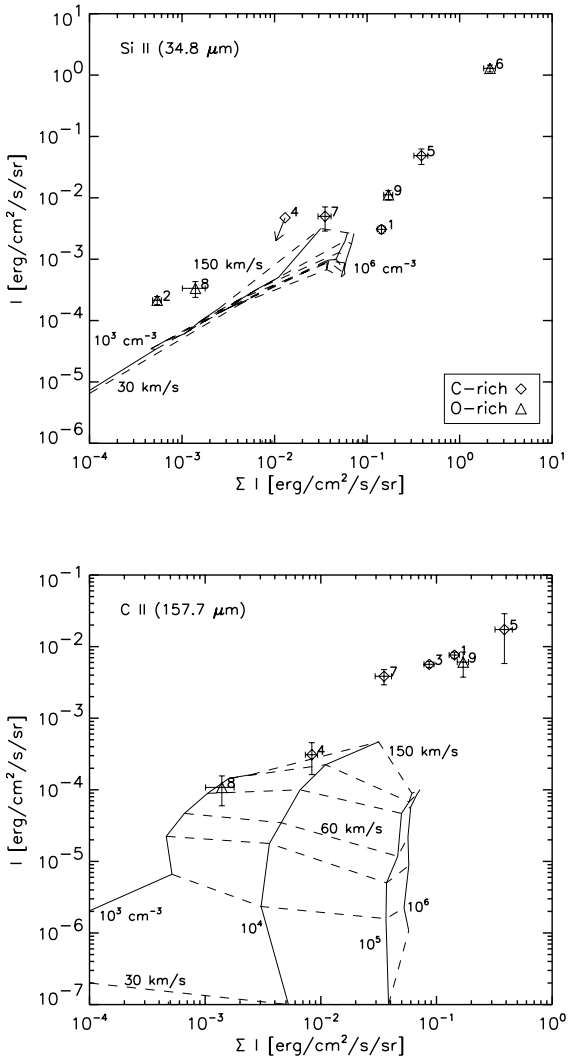

Fig. 6. Comparison of the observed intensities with J-shock model predictions (van den Ancker 1999). Solid lines are values for constant density and dashed lines of constant velocity. On the x-axis, ΣI is the sum of all measured lines.

observations with models can be used to distinguish between both mechanisms. Van den Ancker (1999) deduced some useful tips to distinguish the presence of a PDR or a shock (C or J type) by comparing a large sample of objects to PDR and shock models. Among all of them, the criteria relevant for this study are: 1) the detection of [Si II] or [Fe II] implies the presence of a PDR or a J-shock respectively. 2) The presence of strong [S I] emission unambiguously indicates that a shock is present.

In six PNe the [Si II] line has been detected (Table 5). This rules out the presence of C-shocks in these nebulae. Since C-shocks are characterized by low degrees of ionization no [C II] is expected. This line has been measured in seven of the PNe, including the three that have no [Si II], and this points to the presence of PDRs or J-shocks. We can therefore rule out the presence of C-shocks in these nebulae. We have plotted the intensities of [Si II] and [C II] with those predicted by J-shock models at different densities and velocities of the shocked gas in Fig. 6. It can be seen that the J-shock models cannot reproduce the observed intensities (including the upper-limit to the Si II line flux in NGC 3918). This comparison together with the fact that in none of the PNe is the [S I] line observed suggests that the gas emitting these fine-structure lines is photo-dissociated and heated by the strong stellar FUV photons rather than by shocks.

Table 7. Molecular intensities corrected for extinction in units of 10^{-4} erg cm^{-2} s^{-1} sr^{-1}.

Transition	λ (μm)	NGC 7027	Hb 5	NGC 6302
1-0Q(1)	2.406	9.26		7.60
1-0Q(3)	2.423	5.82	29.2	3.82
1-0Q(5)	2.455			4.00
1-0O(3)	2.802	7.08	79.2	0.62
2-1O(3)	2.972			0.91
1-0O(4)	3.004	1.39		1.15
1-0O(5)	3.235	1.84		1.44
1-0O(6)	3.501			0.83
0-0S(7)	5.511	5.04	57.9	
0-0S(5)	6.909	14.5	121.4	10.4
0-0S(4)	8.026	5.52	54.1	3.93
0-0S(3)	9.665	15.9	115.0	10.4
0-0S(2)	12.279			8.57
0-0S(1)	17.035	2.87[†]	36.3	7.79

[†] This line was not reported by Bernard Salas et al. (2001) because it was barely seen in their spectrum. It could be detected using the latest calibration files and de-fringing tools currently available in *IA*.

8. H_2 in NGC 7027, Hb 5 and NGC 6302

Molecular hydrogen emission lines have been measured in the SWS spectrum of Hb 5 (this paper), NGC 7027 Bernard Salas et al. (2001) and NGC 6302 Beintema & Pottasch (1999). In particular, pure-rotational 0–0 transitions and ro-vibrational 1–0 transitions were detected for all three nebulae. For NGC 6302 even a ro-vibrational transition 2–1 was detected. Their intensities (corrected for extinction) are listed in Table 7.

The H_2 lines (since they are optically thin) can be used to derive the column density of a certain upper level J. Assuming LTE and using the Boltzmann equation a relation between the total number of molecules $N(H_2)$ and the rotational temperature ($T_{\rm rot}$) is found which can be conveniently expressed in logarithmic form:

$$\ln\left(\frac{N(J)}{g_J}\right) = -\frac{E_J}{kT_{\rm rot}} + \ln(N(H_2)\frac{hcB}{2kT_{\rm rot}}. \quad (2)$$

In this equation, g_J is the statistical weight of the upper level J, E_J the energy levels (from Dabrowski 1984), k the Boltzmann constant and B is the rotational constant. As discussed by van den Ancker et al. (2000), by plotting the $\ln(N(J)/g_J)$ versus the energy of the level the rotational temperature and column density can be derived by fitting a Boltzmann distribution to the pure rotational lines.

This has been done in Fig. 7 for the three nebulae where H_2 data was available. The gas temperatures found (between 500 and 830 K) can be reproduced with the models (i.e. Kaufman et al. 1999). For NGC 6302, the distribution shows a break around $E_J \sim 6000$ K, with evidence for cool and warm

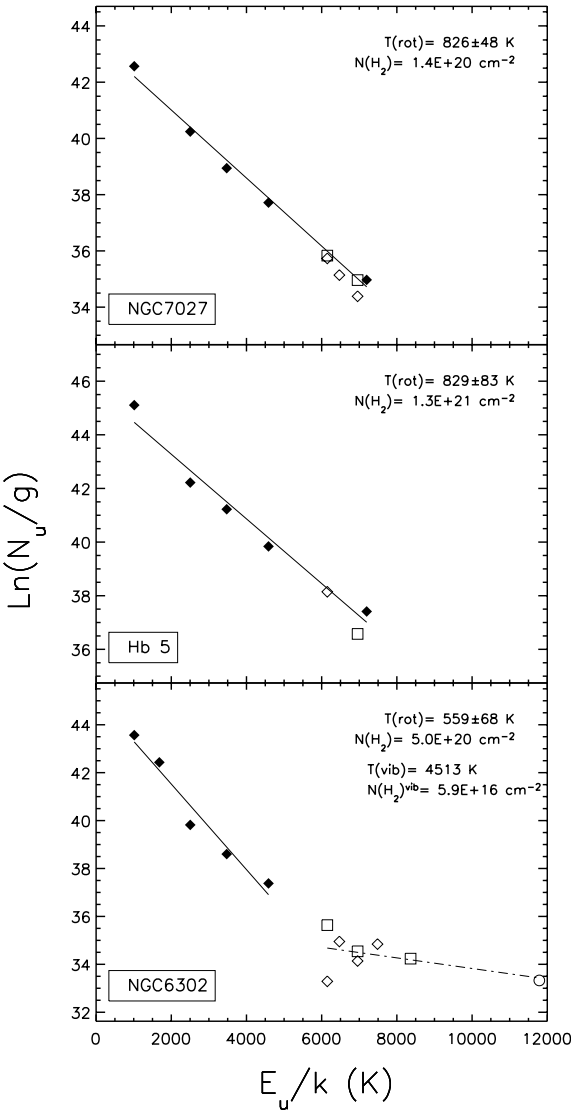

Fig. 7. Molecular hydrogen excitation diagrams for NGC 7027, Hb 5 and NGC 6302. The solid lines represent the Boltzmann distribution fits to the pure rotational lines (solid diamonds) and the dashed dot line is a fit to the vibrational lines in NGC 6302. The symbols represent the different transitions: 0–0S → filled diamonds, 1–0O → Open diamonds, 1–0Q → squares, 2–1O → circle.

gas. Two lines were fitted to this data. The high E-fit is not very accurate since only one line with energy above 9000 K has been measured. This fit has no physical meaning because photo-pumping of H_2 is important and thus the population of the levels starts to deviate from a Boltzmann distribution. Nevertheless, it provides an approximate idea of the conditions in the warmer gas. The results are given in the upper right corner of the figure for each nebula. The difference between the rotational and vibrational temperature in NGC 6302 suggests that photo-dissociation is present. Unfortunately the same cannot be said for the other two nebulae since not enough ro-vibrational lines were detected.

In Fig. 8 the molecular column densities and rotational temperatures of the three nebulae have been plotted together with a sample of young stellar objects dominated by shocks or PDRs.

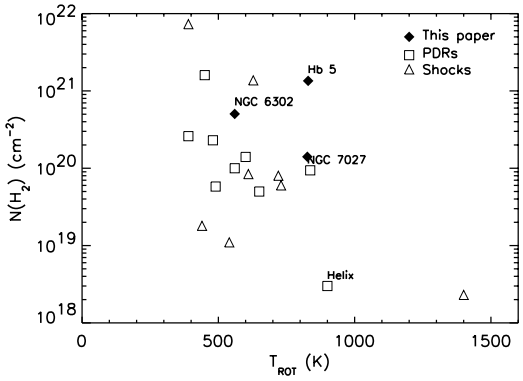

Fig. 8. Comparison of H_2 column density and rotational temperature derived for NGC 7027, Hb 5 and NGC 6302 and a sample of young stellar objects from van den Ancker et al. (2000). The Helix nebula (Cox et al. 1998) is also plotted.

The Helix nebula (Cox et al. 1998) has also been included. The PNe are grouped in a small range of *high* temperatures but expand to a wide range of molecular column densities. The PNe studied by Liu et al. (2001) show PDR temperatures of ∼200–400 K, except in three nebulae that show $T_{\rm rot} >$ 1500 K.

Figure 8 shows that these parameters do not provide good criteria to separate shocked gas from photo-dissociated gas.

9. Atomic, ionized and molecular mass

Atomic, ionized and molecular masses have been derived. The masses depend on the distance and have consequently a large error, but they can be compared to each other since they all depend in the same way (square) on the distance. Furthermore, the molecular masses rely on the assumption that the low J CO lines are optically thin which may not be applicable for all nebulae. In PNe with strong bipolar morphology and where the optical depth is high (because of the torus geometry), some mass could still be self-shielded. However, as we shall see, this seems not to be important.

The atomic mass has been calculated from the [C II] flux using the relation given by Fong et al. (2001) which is described in more detail by Castro-Carrizo et al. (2001). Essentially, for the conditions in the PDRs associated with these PNe, the temperature of the atomic gas is well above the excitation energy of the level involved and the density is much higher than the critical density. Moreover, the [C II] line is expected to be (marginally) optically thin and hence is a good measure for the total mass of gas that is emitting. The main uncertainty is associated with the adopted distances and carbon abundances.

$$M(M_\odot) = 7 \times 10^6\, F(\mathrm{C\,II}) d^2 / X_\mathrm{c}. \quad (3)$$

In Eq. (3) F(C II) is the flux of the 157.7 μm line in erg cm^{-2} s^{-1}, d is the distance in kpc, and X_c is the carbon abundance. This abundance has been taken from the same references as the extinction in Table 2. There is no carbon abundance for Hb 5 and Mz 3 and a value of 4×10^{-4} has been assumed which is probably a good approximation. Fong et al. (2001) include in their equation a correction factor (F_c) which is needed when

Table 8. Atomic, ionized and molecular (hydrogen and CO) masses. In the last column the nebular diameter (see Sect. 10 for details) in arcsec is given.

Name	Masses ($M_\odot$)				Nebular
	atomic	ionized	H_2	mol*	diameter
NGC 7027	0.21	0.018	0.004	0.60	14.2
NGC 6153		0.142			25.0
BD+30 3639	0.07	0.037		0.001	7.5
NGC 3918	0.005	0.072			10.0
Hb 5	0.36	0.112	0.026		20.0
Mz 3		0.091		0.5	25.4
K 3-17	0.18				14.8
NGC 6543	0.01	0.058			18.8
NGC 6302	3.34	0.248	0.038	0.28	10.0

* Molecular masses derived from CO observations (see Sect 9).

the excitation temperature ($T_{\rm ext}$) is low. This factor becomes one when $T_{\rm ext} \gg 92$ K. The rotational temperatures derived in the previous section were much greater than 92 K and we have assumed that it is also probably the same for the other PNe and therefore $F_{\rm c} = 1$.

The ionized mass has been calculated using the Hβ flux. The flux is related to the mass in the following equation:

$$M(M_\odot) = 11.06 F(\mathrm{H}\beta) d^2 \left(\frac{T_{\rm e}}{10^4\ \mathrm{K}}\right)^{0.88} / N_{\rm e}. \quad (4)$$

In this equation the electron density ($N_{\rm e}$) and temperature ($T_{\rm e}$) have been taken again from the same references as the extinction in Table 2 except for Mz 3 where $T_{\rm e}$ and $N_{\rm e}$ have been taken from Quinn et al. (1996). Unfortunately for K 3-17 the mass could not be derived because the Hβ flux is unknown.

Knowing the H_2 column density ($N(H_2)$) and the distance to the object the mass of molecular hydrogen ($M(H_2)$) can be determined using;

$$M(\mathrm{H_2}) = 2\, m_{\rm H}\, \pi \left(d\frac{\theta}{2}\right)^2 N(\mathrm{H_2}) \quad (5)$$

where $m_{\rm H}$ is the mass of the hydrogen nuclei, d being the distance to the nebulae and θ the nebular diameter (see Table 2). Note that this estimate of the molecular hydrogen mass is heavily weighted towards warm molecular hydrogen associated with the PDR.

The atomic, ionized and H_2 masses are given in Table 8. These mass estimates are complemented by molecular masses derived from low J CO observations from the literature. These latter mass estimates are much better probes of the cold molecular gas mass associated with these PNe. The values used are listed in Table 8 and were taken from; Bujarrabal et al. (2001) (NGC 7027), Bujarrabal & Bachiller (1991) (Mz 3), and Huggins et al. (1996) (BD+30 3639 and NGC 6302). Since Huggins et al. (1996) sometimes adopted distances that are different from our values, we have scaled their masses to our assumed distances. They also adopted a CO-abundance of 3×10^{-4}. We have scaled these to the carbon abundance on the oxygen-rich PNe (since the carbon should be in CO), and to the oxygen abundance for the carbon-rich PNe (since the oxygen should be in CO). For NGC 7027 the observed integrated intensity of the ^{12}CO 2–1 transition varies by about a factor 2 even observed with the same telescope (Huggins et al. 1996; Bujarrabal et al. 2001). Likely, this reflects pointing variations between these data sets coupled with the extended nature of this source (Graham et al. 1990). Here we elect to use the higher value of the measurements (Bujarrabal et al. 2001) for the adopted molecular mass (0.6 $M_\odot$). For Mz 3 the observed integrated ^{12}CO 2–1 intensity is very low compared to other sources (Bujarrabal & Bachiller 1991). This would imply a molecular mass of only 0.002 $M_\odot$ (Huggins et al. 1996). This low molecular mass may reflect the effect of UV photodissociation of CO. If following Bujarrabal & Bachiller (1991), we adopt a CO abundance of 5×10^{-7}, a molecular mass of 0.5 $M_\odot$ is derived and this value is used here.

Table 8 shows that the overall mass budget is in general dominated by the atomic mass. However, for NGC 3918 and NGC 6543 the ionized mass is larger than the atomic mass by a factor ~4. This is interesting since it implies that not in all nebulae is the atomic mass larger than the ionized mass, as is often assumed. The derived H_2 mass is in principle representative of the warm molecular region in the PDR (since it is rotationally and vibrationally excited) and not of the total molecular mass. This can be seen in NGC 7027 where the H_2 mass is clearly smaller than the molecular mass. Since for Hb 5 no molecular mass is available, for the discussion in the next section, we have assumed that the H_2 mass is representative of the molecular mass for that nebula. This is probably a lower limit but as we shall see later even a molecular mass of double that assumed does not compromise our conclusions. The atomic mass in NGC 6302 found by Liu et al. (2001) of 0.6 $M_\odot$ is much lower than the value we obtain because they used an erroneous carbon abundance for this nebula.

10. General discussion

An interpretation of the evolution of the different mass components (ionized, atomic and molecular) in the nebulae is given in this section. For that purpose, ratios of masses (to avoid uncertainties in the distances) have been plotted against the nebular radius in Fig. 9. Following Huggins et al. (1996) this radius can be roughly related to the age of the nebula where older nebulae have larger radius than young nebulae. Due to the different morphologies in PNe and in order to be consistent, the nebular radius used is that of the main ionized component in the nebula. In the interaction wind model the size will depend on the geometry. In particular, in bipolar nebulae, the PDR emission may mainly originate in a toroidal region while the optical emission could trace the diffuse extended region. The latter could be a better indicator of the age and, hence, we have adopted (when possible) the optical size here.

These radii have been derived from the diameters labeled in the last column of Table 8 and have been taken from Cahn et al. (1992), except, BD+30 3639 and NGC 6302 (Acker et al. 1992, from optical and radio images, respectively), and NGC 3918 from Corradi et al. (1999).

Unfortunately, the conclusions drawn below are impacted by the small sample of objects and the strong bipolar

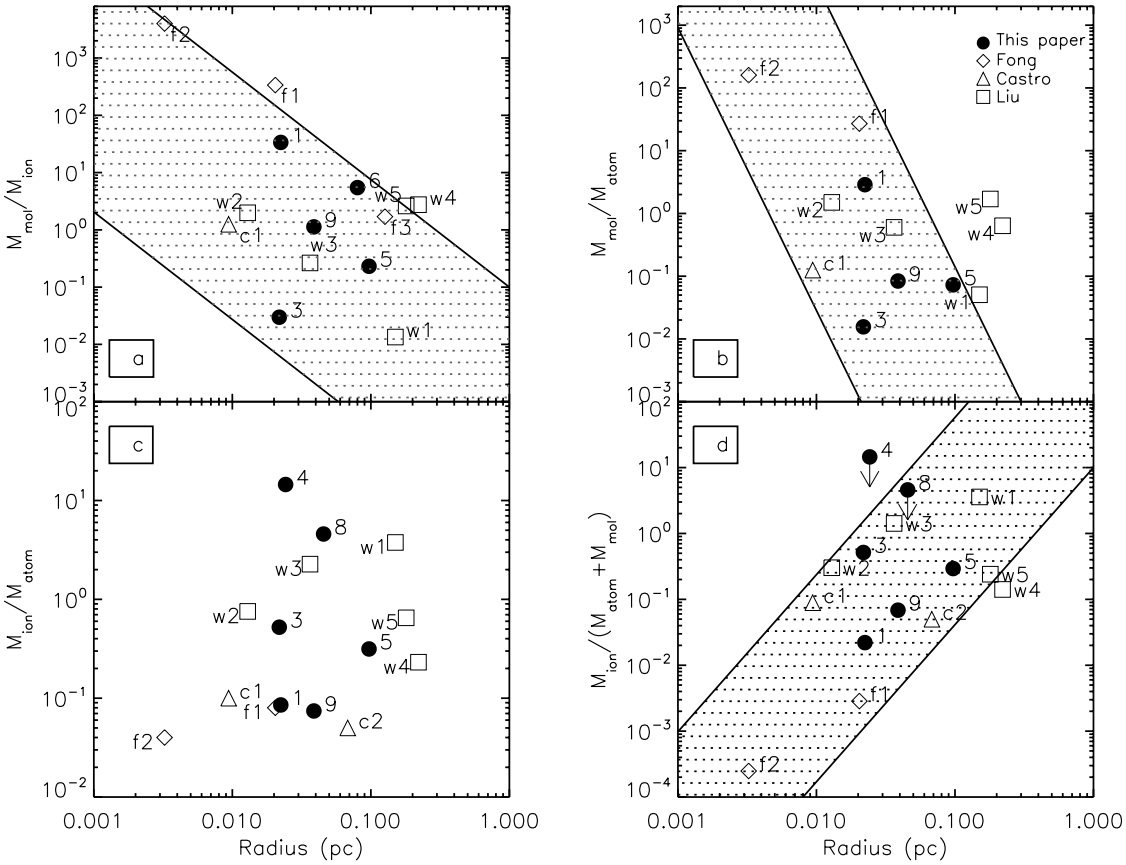

Fig. 9. Ratio of masses plotted against the radius of the nebula. The numbers close to the symbols indicate the sources (see text for details): 1→NGC 7027, 2→NGC 6153, 3→BD+30 3639, 4→NGC 3918, 5→Hb 5, 6→Mz 3, 7→K 3-17, 8→NGC 6543, 9→NGC 6302, f1→IRAS 21282+5050, f2→ AFGL 618, f3→NGC 6720, c1→M 2-9, c2→Hb 12, w1→IC 4406, w2→IC 5117, w3→NGC 3132, w4→NGC 6072, w5→NGC 6781.

geometries exhibited by some of the sources. In addition to the small sample presented, not all the masses (atomic, ionized, and molecular) were always available. For those reasons five PNe from Liu et al. (2001), three PPN/young PNe and two PNe from Fong et al. (2001) and Castro-Carrizo et al. (2001) have been included in the sample. The objects are: PPN/young PNe IRAS 21282+5050 (labeled as f1 in Fig. 9), AFGL 618 (f2) and Hb 12 (c2), and PNe NGC 6720 (f3) and M 2-9 (c1). From Liu et al. (2001) we selected those PNe (assigned with the letter *w* in the figures) where both atomic and molecular masses, diameters and H_β flux were available. For these nebulae we derived the ionic masses using Eq. (4). The electron temperature for these nebulae is not given, and a value of 10 000 K has been assumed (note that the dependence on temperature in Eq. (4) is very small). To derive the radius, the diameters by Cahn et al. (1992) were adopted except for NGC 3139 in which the diameter given by Acker et al. (1992) was used.

In Fig. 9 (a and b) the ratio of the molecular to ionized mass and molecular to atomic mass are shown. The hatched area in Fig. 9a represents approximately the trend seen by Huggins et al. (1996) using a much larger sample of PNe. While our objects by themselves do not show an obvious trend they lie within the trend seen by Huggins et al. (1996). In Fig. 9b the hatched area in the figure is to guide the eye. The ratios show a large spread but also a tendency to decrease with radius. NGC 6072 (labeled w4 in the figure), and NGC 6781 (w5) have large diameters, especially the latter, and some atomic mass may have been missed if not all the [C II] flux was contained within the LWS beam. As the nebula evolves, the material ejected during the Asymptotic Giant Branch phase expands and the total column density through the ejecta will drop (Huggins et al. 1996). As a consequence, the incident FUV flux from the central star can penetrate deeper into the molecular envelope dissociating first and ionizing later more molecules, therefore the ratios $M_{\rm mol}/M_{\rm ion}$ and $M_{\rm mol}/M_{\rm atom}$ decrease. In the figure, the less evolved objects (PPN/young PNe f1 and f2) show the largest ratio while the ratio is lower for the more evolved PNe. The spread seen in Fig. 9c probably reflects that the evolution of the envelope not only depends on the age, but also on the intrinsic properties of the nebulae, such as morphology, progenitor mass, etc. In the last panel of the figure (d), the ratio of the ionized mass to the sum of the atomic and molecular masses is plotted. Again the hatched area simply guides the eye. NGC 3918 (number 4) and NGC 6543 (8) are included but are upper limits because no molecular mass is available and the ratio is therefore only to the atomic mass. There is a trend of increasing ionic mass relative to the atomic and molecular mass with the size of the nebula. Thus, although a significant mass is neutral PDR material, the importance of the ionized material clearly grows as the nebula expands. The reader should bear

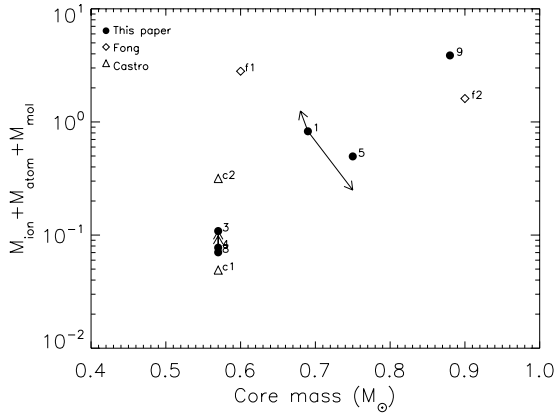

Fig. 10. Sum of nebular masses versus the core mass.

in mind that these relations are limited by the age-size relation assumed in the paper. A larger sample of objects would help in minimizing this uncertainty.

From Fig. 9 (a and b) and Table 8 it can seen that NGC 7027 still has an important reservoir of molecular gas (comparable to the atomic mass) while in NGC 6302 the neutral envelope has been mostly photo-dissociated and is mainly in the neutral atomic form. The latter is interesting. Marigo et al. (2003) concluded that NGC 6302 evolved from a 4.5–5 $M_\odot$ star (this is supported by Fig. 1). Its evolution might have been faster as well, and the material may have been exposed for a shorter period to the FUV flux. The relatively large ionized mass in NGC 3918 (Fig. 9 Table 8) is expected because from the HR diagram (Fig. 1) it is the most evolved object in our sample. On the other hand, NGC 6543 show also a large fraction of ionized mass yet it seems to be in an early phase of PN evolution. Observations of the molecular gas masses for these objects may be an interesting test since we expect a low molecular mass for NCG 3918 and a large one for NGC 6543.

Figure 10 represents the sum of the three masses with respect to the core mass inferred from the HR diagram (Fig. 1). For the objects lying below the evolutionary tracks in the HR diagram the lowest core mass (0.57 $M_\odot$) was adopted. The vertical arrows for NGC 3918 and NGC 6543 indicate that the sum for these objects is a lower limit since no molecular mass was measured. This plot should be used with caution because the parameters plotted strongly depend on the distance. In view of the large uncertainties associated with the quantities shown, there is a good relationship between the total gas mass and the core mass of the PNe. Part of the spread in this relationship may actually reflect the uncertainties in the adopted distances which has the tendency to spread the points perpendicular to the relationship. This is illustrated for NGC 7027 (number 1) where the arrows indicate an error in the distance of a factor of 1.5. This nebula has been thoroughly studied in the literature and its distance is one of the better determined (probably an error lower than 1.5), but it helps to realize how inaccurate the other objects might be. We therefore do not conclude anything firmly from it but we believe that the discussion and suggestions given are worthwhile.

The core mass is related to the progenitor mass. Larger core masses imply larger progenitor masses, and more material is then ejected. This is the trend displayed in Fig. 10. We note that NGC 6302, which is believed to descend from a high mass progenitor ($M > 4.5\ M_\odot$; Marigo et al. 2003), also has the highest total gas mass associated with it. Likewise, NGC 7027 is thought to originate from a star with a mass around 2–3 $M_\odot$ (Middlemass 1990), and has a more modest amount of nebular gas associated with it. A source like NGC 3918 likely had a low mass progenitor (Clegg et al. 1987) and its nebular mass is small. Specifically, adding the atomic, molecular and ionized mass in NGC 6302 a value of 3.9 $M_\odot$ is obtained. This value agrees remarkably well with a progenitor mass of 4–5 $M_\odot$ concluded by Marigo et al. (2003) for this nebula since models predict 4 $M_\odot$ stars to eject ∼3.3 $M_\odot$ (Marigo et al. 1996) at the end of the AGB phase. This progenitor mass is confirmed from the the dust mass derived by Kemper et al. (2002) (0.05 $M_\odot$), since assuming a gas to dust ratio of 100, a 5 $M_\odot$ is found. In contrast, for NGC 7027 we obtain a total mass for the progenitor of only 1.2 $M_\odot$. (Fig. 10), and some of the ejected mass still seems to be missing. Perhaps this reflects the importance of high density molecular gas in the PDR (see Sect. 6.2).

Another important issue is the relation of the dust features (Table 4) to the nucleosynthetic evolution of the progenitor star. We note that a classification of PNe based on arguments of the dust features was made by Zuckerman & Aller (1986). Regardless of the large uncertainties involved we would like to hypothesise the following ideas.

While the MgS dust feature is present, no traces of other dust features have been observed in NGC 3918 (see Table 4) shortwards 12 μm. This C-rich PN has the largest C/O ratio (together with BD+30 3639) and PAH features might have been expected in that part of the spectrum. Although the spectrum is noisy, PAH features such as the 11.2 feature in BD+30 3639 should have been detected at the S/N of the SWS spectrum. This needs to be further investigated. Mz 3 and NGC 6543 show silicate features and together with NGC 3918 no PAHs. Their positions in the HR diagram are different but all point to low core masses, and therefore low progenitor masses. The oxygen-rich nature of the dust ejecta in Mz 3 and NGC 6543 suggests that these objects never experienced enough dredge-up of carbon-rich material to turn the ejecta carbon-rich, and hence their stellar progenitors must have had masses below ∼1.5 $M_\odot$ (Boothroyd & Sackmann 1988). In contrast, Hb 5 and NGC 7027 (see Fig. 10) show emission characteristics for dust condensates formed in carbon-rich ejecta (e.g., PAHs and MgS; Hony et al. 2001, 2002b,a) and hence must have originated from progenitors of an intermediate mass range (∼1.5–4 $M_\odot$, Boothroyd & Sackmann 1988; Vassiliadis & Wood 1993; Marigo et al. 2003). NGC 6302 shows both the presence of silicates and PAH features and the largest core mass (Fig. 10). Marigo et al. (2003) deduced indeed that the progenitor mass of NGC 6302 must have been 4–5 $M_\odot$ and hence that it experienced hot bottom burning (Boothroyd et al. 1995; Vassiliadis & Wood 1993). In this process, carbon is destroyed at the expense of nitrogen, and the star must experience an oxygen-rich phase. In summary, NGC 6302 probably experienced a carbon-rich phase during its evolution, but then with the onset of the hot bottom burning it turned oxygen-rich again. Finally, we note that these estimates based on the dust

characteristics are in good agreement with our stellar mass estimates derived from Fig. 10.

We have left BD+30 3639 out of this discussion. This nebula has a Wolf-Rayet [WC9] central star and exhibits a strong carbon- and oxygen-rich dust chemistry. A recent study of this kind of object has been done by Cohen et al. (2002). The position of BD+30 3639 in the HR diagram (see Fig. 1) does not agree well with the evolutionary tracks, and already suggests a different evolutionary status than a *normal* PNe. It has been suggested that this PN could have experienced the so-called *born again phase*, a late He-shell flash that brings the star back to the AGB phase, this time burning helium instead of H. Alternatively, Górny & Tylenda (2000) have suggested that, more likely, these stars have evolved directly from the AGB and have not experienced a born again phase.

While the relationship between the characteristics of the dust emission features and the nucleosynthetic history of the progenitor stars is tantalizing, because of the uncertainty in the position of the nebulae in the HR diagram, it is too early to draw firm conclusions at this point. Nevertheless, a similar study of PNe in nearby galaxies and/or the galactic center (where the distances are much better known) should be very illuminating.

11. Summary and conclusions

Data of the fine structure lines of [C II] (157.7 μm), [O I] (63.2 and 145.5 μm), and [Si II] (34.8 μm) for nine PNe have been presented.

Since the intensities of [C II], [O I] and [Si II] control the cooling in the photo-dissociation regions a comparison of the observed lines with PDR models has allowed us to derive the densities of these regions. This has been done taking into account the carbon or oxygen rich nature of the PNe. Although current PDR models are created for the ISM (which is oxygen-rich), Latter (2004, as reported in Fong et al. 2001) has developed a new PDR code which properly treats carbon rich environments. Comparison of individual intensities with G_0 allowed us to derive the density of the PDR regions. Some objects lie outside the range predicted by the models (in all the lines studied) and for some others the derived densities show a large spread, especially in the C-rich nebulae. This could be due to uncertainties in the assumed diameter for the PDR, but a comparison of line ratios (avoiding therefore the uncertainty in the diameter) with the models indicate the same problem in the C-rich nebulae. The density in these PNe is probably higher than the critical density and therefore these lines are no longer sensitive to this parameter. We conclude that other species (such as CO) with higher critical densities must be used to derived accurate densities in these PNe.

The absence of the [S I] line at 25 μm in the SWS spectrum (van den Ancker 1999) and a comparison with J-shock models suggests that these lines are heated by the UV radiation field of the central star and not by shocks. Measurements of pure rotational molecular hydrogen lines in NGC 7027, Hb 5, and NGC 6302 have been used to derive the density and rotational temperature of H_2 in the PDR under the assumption of LTE. The rotational temperatures found are high, ~500 to ~800 K.

Atomic, ionized and molecular masses have been derived. We find that the overall mass budget is in general dominated by the atomic mass. Following Huggins et al. (1996) we have assumed that the optical size of the nebula is indicative of the age of the PN. Our results suggest that as the nebula ages, the ionized mass grows at the expense of the atomic and molecular mass. A larger sample would help to strengthen this relation. While the uncertainties are large, there is a good relationship between the total gas mass and the core mass of the PNe, supporting the notion that higher mass progenitors produce more massive envelopes and leave more massive stellar cores.

Acknowledgements. We thank the anonymous referee for careful reading of an earlier version of this manuscript which greatly improved the paper. J. Bernard-Salas is grateful to N. L. Martín-Hernández for reducing some of the LWS spectra. J. Bernard-Salas wants also to thank M. Kaufman, W. Latter and D. Fong for providing respectively the O-rich and C-rich PDR models. F. Molster, D. Fong, J. Cami and S. Hony are thanked for useful discussions. We thank M. J. Barlow, L. B. F. M. Waters, J. M. van der Hulst, S. R. Pottasch, P. R. Wesselius and M. Spaans for carefully reading of the manuscript whose comments have improved this article. IA3 is a joint development of the SWS consortium. Contributing institutes are SRON, MPE, KUL and the ESA Astrophysics Division. This research has made use of the SIMBAD database, operated at CDS, Strasbourg, France.

References

Acker, A., Marcout, J., Ochsenbein, F., Stenholm, B., & Tylenda, R. 1992, Strasbourg - ESO catalogue of galactic planetary nebulae. Part 1; Part 2. Garching: European Southern Observatory
Bains, I., Bryce, M., Mellema, G., Redman, M. P., & Thomasson, P. 2003, MNRAS, 340, 381
Beintema, D. A., & Pottasch, S. R. 1999, A&A, 347, 942
Bernard Salas, J., Pottasch, S. R., Beintema, D. A., & Wesselius, P. R. 2001, A&A, 367, 949
Bernard-Salas, J., Pottasch, S. R., Wesselius, P. R., & Feibelman, W. A. 2003, A&A, 406, 165
Boothroyd, A. I., & Sackmann, I. J. 1988, ApJ, 328, 671
Boothroyd, A. I., Sackmann, I. J., & Wasserburg, G. J. 1995, ApJ, 442, L21
Bujarrabal, V., Castro-Carrizo, A., Alcolea, J., & Sánchez Contreras, C. 2001, A&A, 377, 868
Bujarrabal, V., & Bachiller, R. 1991, A&A, 242, 247
Cahn, J. H., Kaler, J. B., & Stanghellini, L. 1992, A&AS, 94, 399
Castro-Carrizo, A., Bujarrabal, V., Fong, D., et al. 2001, A&A, 367, 674
Ciardullo, R., Bond, H. E., Sipior, M. S., et al. 1999, AJ, 118, 488
Clegg, P. E., Ade, P. A. R., Armand, C., et al. 1996, A&A, 315, L38
Clegg, R. E. S., Harrington, J. P., Barlow, M. J., & Walsh, J. R. 1987, ApJ, 314, 551
Cohen, M., Barlow, M. J., Liu, X. W., & Jones, A. F. 2002, MNRAS, 332, 879
Cohen, M., Kunkel, W., Lasker, B. M., Osmer, P. S., & Fitzgerald, M. P. 1978, ApJ, 221, 151
Corradi, R. L. M., Perinotto, M., Villaver, E., Mampaso, A., & Goncalves, D. R. 1999, ApJ, 523, 721
Cox, P., Boulanger, F., Huggins, P. J., et al. 1998, ApJ, 495, L23
Dabrowski, I. 1984, Canadian J. Phys., 62, 1639
de Graauw, T., Haser, L. N., Beintema, D. A., et al. 1996, A&A, 315, L49

Ercolano, B., Morisset, C., Barlow, M. J., Storey, P. J., & Liu, X. W. 2003, MNRAS, 340, 1153
Fong, D., Meixner, M., Castro-Carrizo, A., et al. 2001, A&A, 367, 652
Górny, S. K., & Tylenda, R. 2000, A&A, 362, 1008
Graham, J. R., Matthews, K., Neugebauer, G., et al. 1990, BAAS, 22, 813
Habing, H. J., 1968, Bull. Astr. Inst. Netherlands, 19, 421
Hollenbach, D., & McKee, C. F. 1989, ApJ, 342, 306
Hollenbach, D. J., & Tielens, A. G. G. M. 1999, Rev. Mod. Phys., 71, 173
Hony, S., Van Kerckhoven, C., Peeters, E., et al. 2001, A&A, 370, 1030
Hony, S., Bouwman, J., Keller, L. P., & Waters, L. B. F. M. 2002a, A&A, 393, L103
Hony, S., Waters, L. B. F. M., & Tielens, A. G. G. M. 2002b, A&A, 390, 533
Hora, J. L., Deutsch, L. K., Hoffmann, W. F., Fazio, G. G., & Shivanandan, K. 1993, ApJ, 413, 304
Huggins, P. J., Bachiller, R., Cox, P., & Forveille, T. 1996, A&A, 315, 284
Justtanont, K., Barlow, M. J., Tielens, A. G. G. M., et al. 2000, A&A, 360, 1117
Kastner, J. H., Weintraub, D. A., Gatley, I., Merrill, K. M., & Probst, R. G. 1996, ApJ, 462, 777
Kaufman, M.J., Wolfire, M. G., Hollenbach, D. J., & Luhman, M. L. 1999, ApJ, 527, 795
Kemper, F., Molster, F. J., Jäger, C., & Waters, L. B. F. M. 2002, A&A, 394, 679
Kester, D. , 2001, in Legacy of the ISO Mission, ed. L. Metcalfe & M. F. Kessler, ESA SP-481, 29
Latter, W. B., Kelly, D. M., Hora, J. L., & Deutsch, L. K. 1995, ApJS, 100, 159
Li, J., Harrington, J. P., & Borkowski, K. J. 2002, AJ, 123, 2676
Liu, X. W., Storey, P. J., Barlow, M. J., et al. 2000, MNRAS, 312, 585
Liu, X. W., Barlow, M. J., Cohen, M., et al. 2001, MNRAS, 323, 343
Marigo, P., Bernard-Salas, J., Pottasch, S. R., Tielens, A. G. G. M., & Wesselius, P. R. 2003, A&A, 409, 619
Marigo, P., Bressan, A., & Chiosi, C. 1996, A&A, 313, 545
Middlemass, D. 1990, MNRAS, 244, 294
Persi, P., Cesarsky, D., Marenzi, A. R., et al. 1999, A&A, 351, 201
Phillips, J. P., & Mampaso, A. 1988, A&A, 190, 237
Pottasch, S. R. 1983, in Planetary Nebulae, IAU Symp., 103, 391
Pottasch, S. R., Bernard-Salas, J., Beintema, D. A., & Feibelman, W. A. 2003, A&A, 409, 599
Quinn, D. E., Moore, T. J. T., Smith, R. G., Smith C. H., & Fujiyoshi, T. 1996, MNRAS, 283, 1379
Reed, D. S., Balick, B., Hajian, A. R., et al. 1999, AJ, 118, 2430
Sabbadin, F. 1986, A&AS, 64, 579
Sahai, R., & Trauger, J. T. 1998, AJ, 116, 1357
Stasińska, G., & Tylenda R. 1986, A&A, 155, 137
Terzian, Y. 1997, In Planetary Nebulae, IAU Symp., 180, 29
Tielens, A. G. G. M., & Hollenbach, D. 1985, ApJ, 291, 722
van den Ancker, M. 1999, Ph.D. Thesis
van den Ancker, M. E., Tielens, A. G. G. M., & Wesselius, P. R. 2000, A&A, 358, 1035
Vassiliadis, E., & Wood, P. R. 1993, ApJ, 413, 641
Vassiliadis, E., & Wood, P. R. 1994, ApJS, 92, 125
Weingartner, J. C., & Draine, B. T. 2001, ApJ, 548, 296
Wolfire, M. G., Tielens, A. G. G. M., & Hollenbach, D. 1990, ApJ, 358, 116
Zhang, Y., & Liu, X. W. 2002, MNRAS, 337, 499
Zuckerman, B., & Aller, L. H. 1986, ApJ, 301, 772